Origin of the orbital polarization of Co^{2+} in La_2CoTiO_6 and $(LaCoO_3)_1 + (LaTiO_3)_1$: A DFT + U and DFMT study

Alex Taekyung Lee
Department of Applied Physics, Yale University, New Haven, Connecticut 06520, USA

Hyowon Park
Department of Physics, University of Illinois at Chicago, Chicago, Illinois 60607, USA

Sohrab Ismail-Beigi
Department of Applied Physics, Yale University, New Haven, Connecticut 06520, USA

(Received 22 June 2020; revised 23 December 2020; accepted 15 February 2021; published 2 March 2021)

The unequal electronic occupation of localized orbitals (orbital polarization), and associated lowering of symmetry and degeneracy, play an important role in the properties of transition metal oxides. Here, we examine systematically the underlying origin of orbital polarization, taking as exemplar the $3d$ manifold of Co^{2+} in a variety of spin, orbital, and structural phases in the double perovskite La_2CoTiO_6 and the (001) superlattice $(LaCoO_3)_1 + (LaTiO_3)_1$ systems. Superlattices are of specific interest due to the large experimentally observed orbital polarization of their Co cations. Based on first principles calculations, we find that robust and observable orbital polarization requires symmetry reduction through the lattice structure; the role of local electronic interactions is to greatly enhance the orbital polarization.

DOI: 10.1103/PhysRevB.103.125105

I. INTRODUCTION

The intriguing electronic and magnetic properties of transition metal oxides (TMOs) are governed by the electronic states derived from their d orbitals. The associated energy bands lie near the Fermi level, and the electronic and magnetic properties of TMOs are strongly dependent on the symmetry and degeneracy of the active d orbitals. High-temperature superconductivity in cuprates [1–4], phase transitions in manganites [5–8], metal-insulator transitions in titanates, vanadates, double perovskites [9–11], and spin-state transitions in cobaltates [12,13] provide classic examples. The degree of broken orbital degeneracy and resulting net differences in orbital populations on the transition metal sites across the unit cell of the material, termed "orbital polarization," is an important ingredient and the focus on this work.

Understanding the properties of TMOs is complicated because the charge, orbital, spin, and lattice degrees of freedom are strongly coupled [6,14] and the physical properties of and phase transitions in TMOs derive from a combination of these couplings. Orbital polarization can be induced by electron-electron (e-e) or electron-lattice (e-l) couplings separately or by mixture of the two. Disentangling the e-e and e-l effects on the orbital properties in real materials is challenging, since both mechanisms result in orbital polarization/ordering and concomitant lattice distortions. In addition, there are many modes for e-l coupling in TMOs such as local Jahn-Teller (JT) distortions or oxygen octahedral tilts and rotations.

Describing the connection between local orbital occupations and orders, local atomic-scale structure, and electron-electron interactions has a rich and long history in condensed matter physics. Many of the classic findings form the cornerstone of the general thinking of this subfield: e.g., Jahn-Teller distortions [15], Goodenough-Kanamori rules for intersite interactions [16–18], Kugel'-Khomskiĭ analysis of magnetic couplings [19], etc. In terms of particular examples, the metal-insulator transition of Fe_3O_4 $\sim$ 120 K is explained by a symmetry-lowering charge ordering with concomitant structural phase transition [20–22]. Additionally, the material shows transitions between ferroelectric and paraelectric phases. The charge order and polarization connect directly to local structural perturbations, and the relation of local structure to electronic and magnetic properties has been elucidated previously [23,24]. Another example involves the orbital polarization of $La_{1-x}Sr_xMnO_3$ manganites which has been studied extensively [6–8,25,26] in terms of the strength of the Jahn-Teller distortion and the hole doping level (x).

However, how one should create orbital polarization from a *materials engineering* viewpoint is not clearly addressed in the literature. What material structure is necessary to create strong orbital polarization? Should one focus primarily on lattice symmetry lowering or strong electronic interactions, and are electronic interactions alone sufficient to create strong orbital polarization spontaneously?

Disentangling the various possibilities is not trivial since prior work focuses on materials in their most stable ground state structures where all the factors act simultaneously. For example, in our prior work, we have engineered and characterized systems with strong orbital polarization in nickelate

and cobaltate superlattices [27–29]. However, since the superlattice geometry automatically breaks structural symmetry, the separate effects and relative importance of (i) structure, (ii) symmetry reduction, and (iii) electronic interactions is unclear. As a typical example, a Jahn-Teller (JT) distortion in a bulk material breaks orbital degeneracy, but it distorts the structure and reduces symmetry at the same time. In contrast, if one forms an oxide superlattice but enforces the local atomic-scale structure to have perfect cubic symmetry, the system already lowers its symmetry from cubic to tetragonal even before any JT distortion appears.

Here, we focus on Co cations in TMOs as exemplar systems where strong orbital polarization can be engineering and observed. Co cations can have multiple spin states, and separately can have active (open-shell) t_{2g} or e_g orbitals depending on their spin state and valence. Bulk $LaCoO_3$ (LCO) containing Co^{3+} is well known for having multiple spin states: It is a low-spin (LS) state (t_{2g}^6, $S = 0$) nonmagnetic insulator at low temperatures [12,30], a paramagnetic insulator for temperatures between 100 and 500 K with either a high-spin (HS) state ($t_{2g}^4 e_g^2$, $S = 2$) [31,32] or an intermediate spin (IS) state ($t_{2g}^5 e_g^1$) [12,33–36], and is metallic above 500 K. However, the orbital polarization of both the HS and LS states of Co^{3+} is zero in $LaCoO_3$ due to its high symmetry.

Recently, we have found remarkably strong orbital polarization of Co^{2+} in $LaCoO_3$+$LaTiO_3$ (LCO+LTO) superlattices [29]. Similar to Co^{3+}, Co^{2+} has multiple spin states but is missing the IS state so only HS ($t_{2g}^5 e_g^2$) and LS ($t_{2g}^6 e_g^1$) are relevant. While the orbital polarization is mainly due to the *minority spin* t_{2g} orbitals for the HS state, the polarization for the LS state is due to the *majority spin* e_g bands. Therefore, this material provides a single system where multiple types of orbital polarization can be studied. We note that strong orbital polarization can also be engineered in nickelate superlattices in a similar fashion [27,28].

In this work, we use first principles electronic structure calculations based on DFT+U theory [37] as well as dynamical mean field theory (DMFT) [13] to study these TMO systems. We elucidate the origin of orbital polarization in both e_g and t_{2g} manifolds and disentangle the role of *e-e* and *e-l* couplings.

We note that "orbital polarization" and "orbital ordering" are related but distinct physical concepts. Orbital polarization is simply the net difference in orbital populations on the transition metal sites averaged across the unit cell of the material. Orbital ordering refers to a periodic pattern of orbital occupations on the transition metal sites that may or may not alternate across the unit cell. For example, ferro-orbital ordering occurs when all transition metal sites show the same pattern of orbital occupancies (in the literature, this is often not considered as a case showing orbital ordering). An antiferro-orbital ordering, more commonly referred to as orbital ordering, shows a staggered alternating pattern in the unit cell.

In this work, to avoid unnecessary complexity, we will be discussing Co^{2+} sites which have identical (or extremely similar) orbital occupations (i.e., ferro-orbital ordering) which makes for a cleaner analysis. However, the ferro-orbital nature of these configurations is the output of the first principles calculations and not due to imposed constraints.

II. COMPUTATIONAL DETAILS

A. Structures and DFT+U

We use density functional theory (DFT) with the projector augmented wave (PAW) method [38] and the revised version of the generalized gradient approximation (GGA) proposed by Perdew *et al.* (PBEsol) [39] as implemented in the VASP software [40]. In all cases, the spin-dependent version of the exchange correlation functional is employed. A plane wave basis with a kinetic energy cutoff of 500 eV is used. We study the (001) $(LaCoO_3)_1 + (LaTiO_3)_1$ superlattice, denoted as LCO+LTO below.

In this work, we use the Glazer notation [41] to describe the rotation and tilting of the oxygen octahedra surrounding the transition metal sites. For the high symmetry structure with $a^0a^0a^0$ octahedral tilts in Glazer notation (i.e., no oxygen octahedron tilts or rotations), corresponding to the $Fm\bar{3}m$ and P_4/mmm space groups, we used 10 atom unit cells (i.e., a (1×1) interfacial unit cell). We used 20 atom unit cells (i.e., $c(2 \times 2)$ interfacial unit cells) for the $a^-a^-b^+$ tilt structure which has the $P2_1/n$ space group. We use Γ-centered **k**-point meshes of size $9 \times 9 \times 9$ ($Fm\bar{3}m$) and $13 \times 13 \times 7$ (P_4/mmm) for the 10 atom cells and $9 \times 9 \times 7$ for the 20 atom cells. For more precise calculations of the energy differences listed in Table I, we used a kinetic energy cutoff of 700 eV and $17 \times 17 \times 17$ **k**-point meshes. The GGA+U scheme within the rotationally invariant formalism together with the fully localized limit double-counting formula [37] is used to study the effect of electron interactions.

Atomic positions within the unit cells were relaxed until the residual forces were less than 0.01 eV/Å. For cases with reduced symmetry, the stress was relaxed only along the z axis to be below 0.02 kB, while the in-plane lattice parameters a and b were set equal and took the values 3.811, 3.851, or 3.891 Å in order to simulate the realistic experimental situation where the superlattice is grown as an epitaxial thin film on a substrate. For the double perovskite La_2CoTiO_6, we used a face-centered cubic unit cell containing 10 atoms, and the lattice parameters correspond to 3.891 Å. We note that 3.891 Å is obtained by minimizing all stresses with $U_{Ti} = U_{Co} = 3$ eV. We consider both ferromagnetic and antiferromagnetic spin orders, however, for simplicity, we focus on the ferromagnetic case unless specified.

The electronic and structural properties depend critically on the U_{Co} value used for the Co $3d$ manifold, and we explore a range of values. We also explore how the results depend on U_{Ti}, which plays a secondary but still important role in the physics of these materials. In this work, we do not employ a Hund's J parameter for any atom in our DFT+U calculations. As explained by prior work, (i) our spin-dependent PBE DFT exchange-correlation functional already describes a sizable exchange interaction prior to including any +U correction, and (ii) further inclusion of a J atop a spin-dependent functional can lead to unexpected (and/or incorrect) physical behavior in a number of transition metal oxides [42–44]. Separately, we are able to obtain and describe the low-spin and high-spin states for Co with $J = 0$ without difficulty.

Since the spin-orbit interactions for $3d$ transition metal atoms are weak, we do not include spin-orbit coupling (SOC) in our calculations and expect their inclusion to lead to only

small quantitative changes. Explicit testing shows only a ≈ 1% difference between orbital occupancies from GGA+U vs GGA+U+SOC (see Appendix A).

Projected density of states are obtained by the spherical harmonic projections inside spheres around each atom. Wigner-Seitz radii of 1.323 and 1.302 Å were used for the projection of Ti and Co atoms, respectively, as implemented in the VASP-PAW pseudopotential. Density matrices for the Co 3d manifold are computed using projector functions based on the PAW methodology as implemented in VASP, following existing frameworks [45,46]. Core radii for projector operators of Ti and Co are 1.357 and 1.249 Å, respectively.

B. DFT+DMFT

We employ the non-charge-self-consistent DFT+DMFT method [13,47] for structures obtained from DFT+U calculations for La_2TiCoO_6 and LTO+LCO with lattice parameter 3.891 Å. We solve the many-body problem only on the manifold of Co 3d Wannier orbitals that describe the Co-derived conduction bands: Physically, these are the states that show broken orbital symmetry. The DFT+DMFT calculation has the following steps. First, we solve the non-spin-polarized Kohn-Sham (KS) equation within DFT+U using VASP. Second, we construct a localized-basis Hamiltonian for the Co 3d bands by generating maximally localized Wannier functions (MLWFs) [48] for the nonmagnetic DFT+U band structure. In both steps, we use $U_{\mathrm{Ti}} = 8$ eV and $U_{\mathrm{La}} = 5$ eV to ionize the Ti and minimize the La d-Co d hybridization, respectively. Finally, we solve the DMFT self-consistent equations for the correlated subspace of Co 3d Wannier orbitals using the continuous time quantum Monte Carlo (CTQMC) [49,50] impurity solver.

Both Hubbard U and Hund's couplings J are parameterized by the (F^0, F^2, F^4) Slater integrals, using $U = F^0$ and $J = (F^2 + F^4)/14$. Only Coulomb interaction matrix elements of the density-density types are considered in the CTQMC while the spin-flip and pair-hopping terms are neglected. We note that the cartesian axes of the Wannier orbitals and the directions of the Co-O bonds are found to be parallel, so that the off-diagonal terms in the d Hamiltonian are negligible. Therefore, the off-diagonal terms in the DMFT hybridization function are neglected during the CTQMC calculation.

For the DMFT calculations, we used U values of 3 and 6 eV and J of 0.5 and 0.9 eV. Here we focus on $U = 3$ eV, which provides a bulk band gap ∼1 eV for $LaCoO_3$ as per prior DMFT work [51]. The two values of Hund's coupling J allow us to obtain the low-spin and high-spin states of Co^{2+} in the DMFT calculations (by tuning the relative strength of the Hund's coupling relative to the crystal field). Specifically, the low-spin state is stable when $J = 0.5$ eV, and the high-spin state is obtained when $J = 0.9$ eV. The J dependence of the Co^{2+} spin state is similar to that of Co^{3+} in bulk $LaCoO_3$ [51]. We used electronic temperatures of 150 K and 300 K to study the temperature effect on the spectral function. Since the results are qualitatively very similar, 300 K results will be discussed unless specified otherwise.

In terms of double counting corrections for DFT+DMFT, we use a double counting energy (E^{DC}) and potential ($V^{\mathrm{DC}} = \partial E^{\mathrm{DC}}/\partial N_d$) similar to the conventional fully localized limit [13,52]:

$$E^{\mathrm{DC}} = \frac{U}{2} N_d \cdot (N_d - 1) - \frac{J}{4} N_d \cdot (N_d - 2)\,, \tag{1}$$

$$V^{\mathrm{DC}} = U\left(N_d - \frac{1}{2}\right) - \frac{J}{2}(N_d - 1)\,, \tag{2}$$

where N_d is the 3d occupancy obtained self-consistently at Co correlated site.

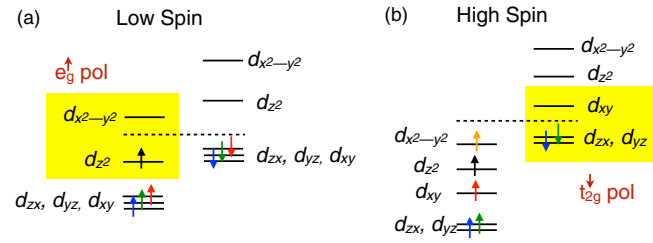

FIG. 1. Schematics energy levels of Co^{2+} ions in $(LaCoO_3)_1 + (LaTiO_3)_1$ superlattices with majority spin up for (a) low-spin state with e_g orbital polarization and (b) high-spin state with t_{2g} orbital polarization. This schematic picture holds for both $P4/mmm$ and $P2_1/n$ phases. The yellow shaded states are those determining the orbital polarization in each case.

III. ORBITAL POLARIZATION OF Co^{2+}

A. LS and HS states: Basics

We begin with a discussion of the basic electronic and magnetic properties of LCO+LTO superlattices which is summarized in our previous studies [29,53]. In LCO+LTO superlattices as well as the double perovskite La_2CoTiO_6, there is a charge transfer from $Ti^{3+}(d^1)$ to $Co^{3+}(d^6)$, resulting in $Ti^{4+}(d^0)$ and $Co^{2+}(d^7)$. The role of electron transfer between Ti and Co has been discussed in prior work [29].

We now highlight some basic facts about the Co^{2+} spin states in the systems studied here. Since the electronic structure of Co^{2+} is strongly dependent on the crystal structure, in this subsection we will focus only on the $P2_1/n$ phase of the superlattice, which is the most stable phase we have found [29,53].

The LS state ($t_{2g}^6 e_g^1$) has $S = 1/2$ and is illustrated by Fig. 1(a): The t_{2g} states are fully occupied, while the one remaining electron is in the e_g channel. In the superlattice, the degeneracy of the e_g manifold is already broken at $U_{\mathrm{Co}} = 0$ due to interface formation and epitaxial strain, with a lower energy d_{z^2} band and higher energy $d_{x^2-y^2}$ band. When $U_{\mathrm{Co}} \geqslant 1.5$ eV, the e_g bands completely split in energy, resulting in an insulating phase: Only the spin-up d_{z^2} is filled in the LS state while the spin-up $d_{x^2-y^2}$ and spin-down e_g bands are empty (see Appendix B for associated densities of states). As a result, the LS state has strong e_g orbital polarization: We find that the polarization is nonzero at $U_{\mathrm{Co}} = 0$, and $U_{\mathrm{Co}} > 0$ simply enhances it.

The HS state ($t_{2g}^5 e_g^2$) with $S = 3/2$ is depicted in Fig. 1(b): The spin-up d bands are fully occupied, while spin-down d bands have two electrons in the t_{2g} channel. Unlike the LS state, the HS state is not even metastable if $U_{\mathrm{Co}} < 1$ eV. When

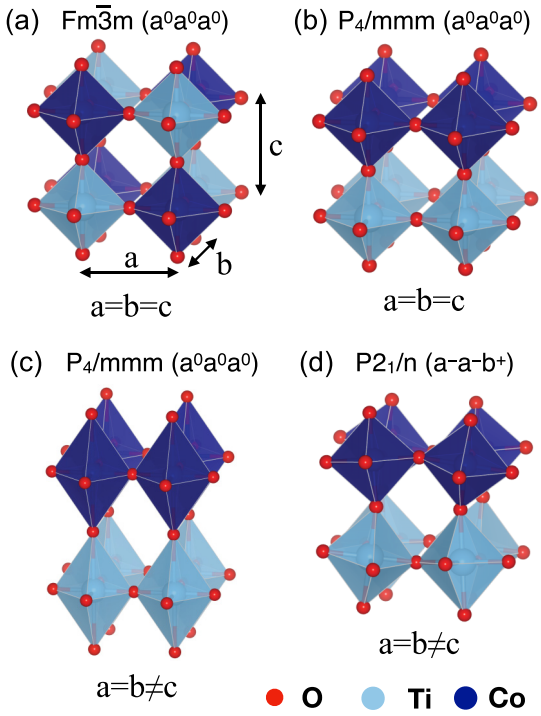

FIG. 2. Schematics of the atomic-scale structures of structures studied in this work. Each structure is labeled by its space group and octahedral rotation pattern. (a) Ideal La_2CoTiO_6 double perovskite. (b), (c), and (d) show one repeat of LCO+LTO (001) superlattices where the (001) direction is vertical. La atoms are not shown for clarity.

$U_{Co} = 1$ eV, the t_{2g} bands split into two nearly-degenerate bands (d_{xz} and d_{yz}) and a single d_{xy} band (see Appendix B for the relevant densities of states.). We note that d_{xz} and d_{yz} are degenerate for the tetragonal phase ($P4/mmm$), but this degeneracy is broken in the monoclinic phase ($P2_1/n$). For $1.5 \leqslant U_{Co} < 2.5$ eV, the d_{xy} band is completely split in energy from the d_{xz}/d_{yz} bands. However, the spin-down d_{xy} band is partially occupied and the spin-up $d_{x^2-y^2}$ band is partially empty, thus the system remains metallic. When $U_{Co} \geqslant 2.5$ eV, the spin-down d_{xy} becomes empty, and the spin-up $d_{x^2-y^2}$ band is fully occupied, resulting in an insulating phase (see Appendix B for relevant densities of states).

B. Structural phases

The e_g polarization of the LS state and the t_{2g} polarization of the HS state can be due to *e-e* and/or *e-l* coupling. To disentangle the effect of these two interactions on the orbital polarization, we consider and compare several reference lattice structures as presented in Fig. 2. As the figure shows, a, b are the in-plane and c the out-of-plane lattice parameters for our systems (the Glazer notation for oxygen octahedral rotations and tilts uses the letters a, b, c but always with a superscript of $0, +, -$ which easily distinguishes the two from each other). (a) We start with the ideal double perovskite La_2CoTiO_6, which has the $Fm\bar{3}m$ space group and no octahedral distortions [Fig. 2(a)] and where $a = b = c$ and the atomic positions are frozen at ideal cubic perovskite coordinates. (b) Next, we have a $(LaCoO_3)_1 + (LaTiO_3)_1$ superlattice obtained by swapping half the Ti and Co in the ideal double perovskite to create a layered superlattice while keeping idealized atomic coordinates and lattice parameters [this has the $P4/mmm$ space group; see Fig. 2(b)]. (c) Another $P4/mmm$ phase superlattice where only the atomic positions and the stress along the c axis are relaxed [see Fig. 2(c)]. (d) Finally, a $P2_1/n$ phase of the LCO+LTO superlattice which has the $a^-a^-b^+$ type of octahedral tilt [41] and is the ground state of the superlattice. The $P2_1/n$ phase is monoclinic, but since we have assumed the epitaxial strain condition where $a = b \neq c$, this differs from a generic monoclinic structure where $a \neq b \neq c$.

In prior work, we found that the charge disproportion and concomitant bond length disproportion can be stabilized in bulk $LaCoO_3$ with nonzero U_{Co} [13,53]. Such disproportionation has important effects on the electronic structure of the Co and can induce a site-selective Mott transition in the other transition metal oxide systems [54–56]. However, we do not obtain such disproportionated phase in $(LaCoO_3)_1 + (LaTiO_3)_1$ or $(LaCoO_3)_2 + (LaTiO_3)_2$ superlattices, although, in principle, the low symmetry of the $P2_1/n$ structural phase permits bond length disproportionation of CoO_6 octahedra. We believe that the underlying reason for the lack of disproportionation is that the Ti has the ionized d^0 configuration: There is no energy lowering drive to lower the energy by further distorting the TiO_6 octahedra. Even if the CoO_6 octahedra wish to disproportionate, they would end up distorting their nearest neighbor TiO_6 octahedra which is energetically costly.

C. LS state: e_g orbital polarization

In this subsection, we focus on the low-spin (LS) state which can have e_g orbital polarization. We note that we find zero or insignificant antiferro-orbital ordering or associated robust JT distortions for the in-plane Co-O bonds in any of the LS phases we considered: For the $Fm\bar{3}m$ and $P4/mmm$ phases the high degree of symmetry precludes it, while for the $P2_1/n$ phase we find negligible (<0.002 Å) such distortions. Separately, out-of-plane Co-O bonds can have JT distortion in the $P4/mmm$ and $P2_1/n$ phases but this does not give rise to antiferro-orbital ordering either.

We define the orbital polarization of the LS state as

$$P(e_g) = \frac{(n^{\uparrow}_{z^2} + n^{\downarrow}_{z^2}) - (n^{\uparrow}_{x^2-y^2} + n^{\downarrow}_{x^2-y^2})}{(n^{\uparrow}_{z^2} + n^{\downarrow}_{z^2}) + (n^{\uparrow}_{x^2-y^2} + n^{\downarrow}_{x^2-y^2})}, \tag{3}$$

where the occupancy n^{σ}_i is the electron population of orbital i with spin σ which is found on the diagonal elements of the single particle density matrix in the Co $3d$ manifold. Figures 3(a)–3(d) present the DFT+U-calculated orbital polarization $P(e_g)$ for the four different structural phases in the LS state as a function of U_{Co} and U_{Ti}.

1. LS $Fm\bar{3}m$ state: Lack of orbital polarization

We begin our analysis with the $Fm\bar{3}m$ space group La_2CoTiO_6 double perovskite structure [Figs. 2(a) and 3(a)]. While P for the $Fm\bar{3}m$ is zero for $U_{Co} \leqslant 1$ eV, it becomes significant for $U_{Co} \geqslant 2$ eV. This happens because of

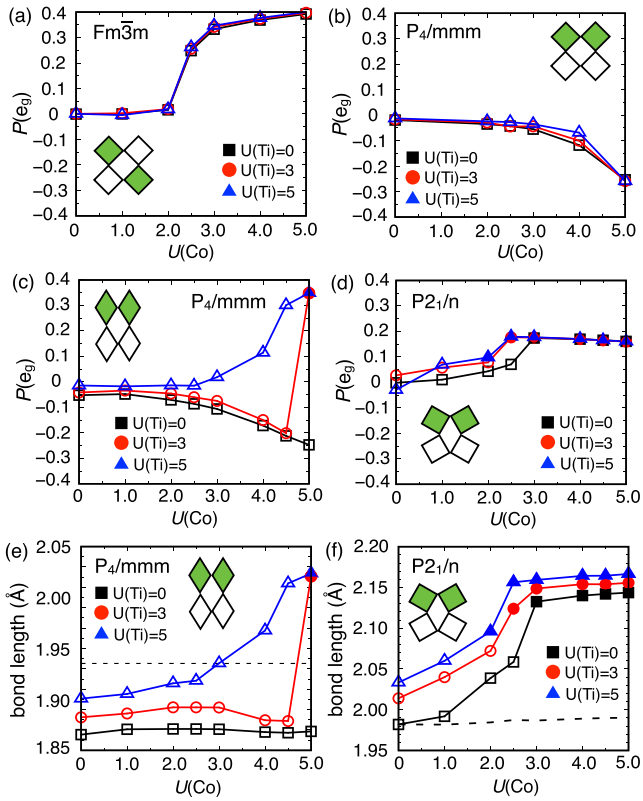

FIG. 3. (a)–(d) show the DFT+U orbital polarization $P(e_g)$ of the LS state structures with different space groups versus U(Co) and as a function of U(Ti). Empty and filled points indicate metallic and insulating phases, respectively. Insets show schematic side views of the octahedral tilts and distortions of the CoO_6 and TiO_6 oxygen octahedra. (e) and (f) present Co-O bond lengths along the c axis of the $P4_1/mmm$ and $P2_1/n$ phases, respectively. Dashed lines represent in-plane Co-O bond lengths which depend weakly on U.

spontaneous electronic symmetry breaking: For large enough U_{Co}, the DFT+U total energy is lowered by having the e_g electron occupy one of the two e_g orbitals more than the other.

However, $P \neq 0$ for $Fm\bar{3}m$ does not necessarily indicate an actual nonzero orbital polarization in the true interacting system because a single-determinant DFT+U description cannot capture the fluctuations between the $d^1_{z^2,\uparrow}$ and $d^1_{x^2+y^2,\uparrow}$ configurations. But, the total energies of the two separate configurations should be well captured by DFT+U. Table I shows that these two configurations are essentially degenerate in energy for $Fm\bar{3}m$ (a fully converged DFT+U calculation should find them exactly degenerate): The degeneracy means that we should expect fluctuations and zero mean orbital polarization in a beyond band theory description of this system. In other words, the DFT+U broken symmetry solution for $Fm\bar{3}m$ is physically incorrect.

We explicitly verify the artificial nature of the DFT+U broken symmetry by performing DFT+DMFT calculations on the $Fm\bar{3}m$ phase with $a = 3.891$ Å in the paramagnetic phase. We use $U = 3$ eV which reproduces the energy gap of bulk $LaCoO_3$ [51]. Orbitally resolved DFT+DMFT spectral functions of the Co d Wannier orbitals in the LS $Fm\bar{3}m$ structure are presented in Fig. 4. We use $J = 0.5$ eV to obtain

TABLE I. Energy difference (in meV/Co) from DFT+U between different Co configurations in the same structure with $U_{\mathrm{Ti}} = 3$ eV and $U_{\mathrm{Co}} = 5$ eV. The configurations are written assuming majority up spin electrons, and only the occupancy of the orbitals of interest are shown. E.g., for the LS e_g case, the full configuration corresponding to the nomenclature $d^1_{z^2,\uparrow}$ is $d^6_{t_{2g}} d^1_{z^2,\uparrow}$. For $Fm\bar{3}m$, $d^1_{xy,\downarrow}(d_{xz,\downarrow}/d_{yz,\downarrow})^1$ means that either the $d_{xz,\downarrow}$ or $d_{yz,\downarrow}$ is filled for all Co cations. For $P4_1/mmm$, $d^1_{xy,\downarrow}(d_{xz,\downarrow}/d_{yz,\downarrow})^1$ means checkerboard (antiferro) orbital ordering and alternating $d^1_{xz,\downarrow}$ and $d^1_{yz,\downarrow}$ Co occupations.

Structure	LS e_g		HS t_{2g}	
	$d^1_{z^2,\uparrow}$	$d^1_{x^2-y^2,\uparrow}$	$d^1_{xz,\downarrow} d^1_{yz,\downarrow}$	$d^1_{xy,\downarrow}(d_{xz,\downarrow}/d_{yz,\downarrow})^1$
(i) $Fm\bar{3}m$	0	0.7	0	0.1
(ii) $P4_1/mmm$ $(a = b = c)$	0	−30	0	66
(iii) $P4_1/mmm$ $(a = b \neq c)$	0	21	0	150

the LS Co^{2+} state (the HS state is not stable with small J, much like Co^{3+} in bulk $LaCoO_3$). We show the DFT+DMFT electronic occupation N_d of Co d Wannier orbitals in Table II.

For the LS $Fm\bar{3}m$ phase of La_2CoTiO_6, Fig. 4(a) and Table II show clearly that the e_g bands are degenerate and equally occupied due to quantum fluctuations of electronic occupancy between d_{z^2} and $d_{x^2-y^2}$. Therefore, the multideterminant nature of the actual ground state washes out the e_g orbital polarization of the single-determinant DFT+U predictions.

2. LS $P4_1/mmm$ and $P2_1/n$ states

Next, we consider the $P4_1/mmm$ superlattice with $a = b = c$ [Figs. 2(b) and 3(b)]. In this phase, the nearest neighbor environment of each Co is still perfectly cubic just as for the $Fm\bar{3}m$ phase, but the global cubic symmetry is broken by

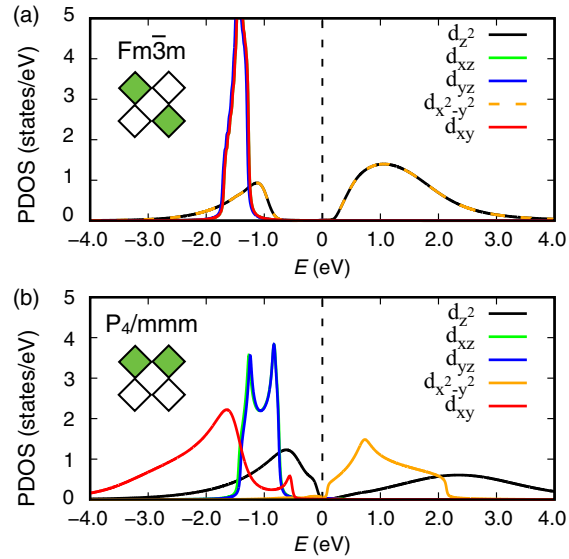

FIG. 4. DFT+DMFT spectral functions of Co d Wannier orbitals for the low-spin state: (a) La_2CoTiO_6 ($Fm\bar{3}m$ structure) and (b) LTO+LCO superlattice ($P4_1/mmm$, $a = b = c$ structure). The calculations use $U = 3$ eV, $J = 0.5$ eV, and a temperature of 300 K.

TABLE II. Co d Wannier occupancies N_d for the low-spin states within DFT+DMFT calculations. The calculations use $U = 3$ eV, $J = 0.5$ eV, and a temperature of 300 K.

	d_{z^2}	$d_{x^2-y^2}$	d_{xy}	d_{xz}	d_{yz}
(i) $Fm\bar{3}m$ La_2CoTiO_6	0.5	0.5	2.0	2.0	2.0
(ii) $P4/mmm$ LCO+LTO ($a = b = c$)	1.0	0.0	2.0	2.0	2.0

the formation of the superlattice along (001). Therefore, the two e_g bands are no longer degenerate even at $U_{\mathrm{Co}} = 0$ (see Appendix B for relevant densities of states). Clearly, $U_{\mathrm{Co}} \neq 0$ is not a *necessary* condition to split the e_g degeneracy: As expected, symmetry reduction by forming a superlattice is enough, but $U_{\mathrm{Co}} > 0$ enhances the magnitude of P substantially. The orbital polarization is small but negative for $U_{\mathrm{Co}} \leqslant 1$ eV but becomes substantially negative once $U_{\mathrm{Co}} \geqslant 2$ eV (i.e., $d_{x^2-y^2}$ is more occupied than d_{z^2}). Table I shows that the $d^1_{x^2+y^2,\uparrow}$ configuration is lower in energy than $d^1_{z^2,\uparrow}$ by 30 meV/Co when $U_{\mathrm{Co}} = 5$ eV: The orbital polarization should survive fluctuations and exist in the interacting realization. We note that for this system, $P(e_g) < 0$ with DFT+U for all U_{Co} considered.

We employ DFT+DMFT calculations for the $P4/mmm$ superlattice with paramagnetic order to verify that the orbital polarization survives with quantum fluctuations. The associated spectral functions are presented in Fig. 4(b) and the Wannier occupancies in Table II. Since the structural symmetry is reduced, the electronic symmetry is broken, the e_g degeneracy is split, and the orbital polarization is evident, all of which is consistent with the DFT+U results.

Interestingly, the d_{z^2} band is lower in energy than the $d_{x^2-y^2}$ band within DFT+DMFT which disagrees with the DFT+U result. The DFT+DMFT result is expected from the Wannier projections: The onsite energy of the d_{z^2} Wannier orbital is 0.50 eV lower than the $d_{x^2-y^2}$ Wannier orbital. Thus, the Wannier d_{z^2} band is already lower in energy than the Wannier $d_{x^2-y^2}$ band at $U = 0$ and increasing U further splits the bands in DFT+DMFT.

On the other hand, the situation with the DFT+U calculations is more complex due to the hybridization of the atomic transition metal d and atomic oxygen p orbitals. If one computes the mean energy of the atomic orbitals using the projected density of states (PDOS) as weights, the atomic d_{z^2} orbitals remain lower in energy than the atomic $d_{x^2-y^2}$, but the actual DFT+U orbital polarization has the opposite sign whereby $d_{x^2-y^2}$ is more occupied. Hence, an explicit treatment of p-d hybridization in the DFT+DMFT calculation will be required to arrive at a complete agreement with DFT+U.

We now move to the $P4/mmm$ phase with $a = b \neq c$ [Figs. 2(c) and 3(c)]. In this structure, the Co ions experience a tetragonal environment due to the relaxation. Similar to the previous $P4/mmm$ $a = b = c$ case, the e_g degeneracy is broken even at $U_{\mathrm{Co}} = 0$, and the polarization magnitude is enhanced by $U_{\mathrm{Co}} > 0$. Most notably, the P for the $P4/mmm$ ($a = b \neq c$) phase can be negative or positive depending on the choices of U_{Co} and U_{Ti} values [see Fig. 3(c)]. While it is clear that U_{Co} changes the splitting of Co 3d bands and also the magnitude

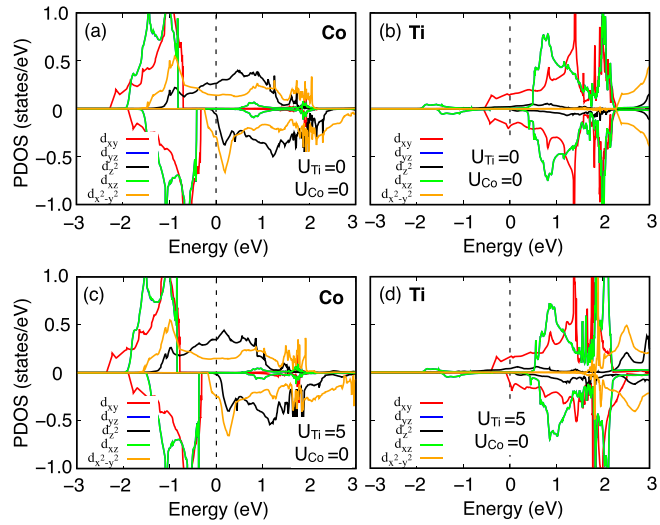

FIG. 5. (a) Co 3d and (b) Ti 3d projected density of states for low-spin (LS) Co in the $(LaCoO_3)_1 + (LaTiO_3)_1$ superlattice with $U_{\mathrm{Ti}} = 0$ and $U_{\mathrm{Co}} = 0$. (c) Co 3d and (d) Ti 3d projected density of states with $U_{\mathrm{Ti}} = 5$ eV and $U_{\mathrm{Co}} = 0$. The in-plane lattice parameters a and b are fixed to 3.891 Å, and the atomic structure has the $P4/mmm$ ($a = b \neq c$) space group.

of P, it is particularly interesting that P also depends strongly on U_{Ti} [compare the three $U_{\mathrm{Co}} = 5$ eV results in Fig. 3(c)].

Since LCO+LTO is a charge-transfer heterostructure, U_{Ti} determines the amount of electron transfer from Ti to Co by adjusting the energy of the Ti 3d orbitals. In detail, a larger U_{Ti} raises the energy of the Ti 3d states and thus forces a larger amount of electron transfer from Ti to Co. Figure 5 shows this point directly: The electron transfer with $U_{\mathrm{Ti}} = 5$ eV is clearly larger than that with $U_{\mathrm{Ti}} = 0$.

Larger transfer induces stronger local electric fields from the TiO_2 to CoO_2 layers, and the field pushes the oxygen anions and increases out-of-plane Co-O bond lengths. The relation between the apical Co-O bond length and P is explained by simple crystal field theory. Long out-of-plane Co-O bonds result in the lowering of the energy of the out-of-plane orbital (d_{z^2}) since O is farther from Co along the c axis, and thus d_{z^2} becomes more occupied and $P > 0$. Conversely, shorter out-of-plane Co-O bonds increase the energy of the d_{z^2} band, so $d_{x^2-y^2}$ becomes more occupied and $P < 0$. We find that when $P < 0$, the Co d bands are always metallic. On the other hand, when $P > 0$ and large enough, the two e_g bands are completely split in energy, and the system is in the insulating regime.

Finally, we consider the $P2_1/n$ phase which is our most stable structural phase. Similar to the $P4/mmm$ ($a = b = c$) and $P4/mmm$ ($a = b \neq c$) phases, $P \neq 0$ at $U_{\mathrm{Co}} = 0$ and increases as a function of U_{Co}. As shown in Fig. 3(d), the P of the $P2_1/n$ phase is always positive, as per our previous work [53]. The d_{z^2} band is significantly lower in energy when $U_{\mathrm{Co}} = 0$ and the material is insulating due to the energy splitting in the e_g manifold (see Appendix B for plots of the densities of states).

The sign of the orbital polarization P is one of the interesting features of our results. Since P can be both positive and negative for the $P4/mmm$ ($a = b \neq c$) phase, it is clear that

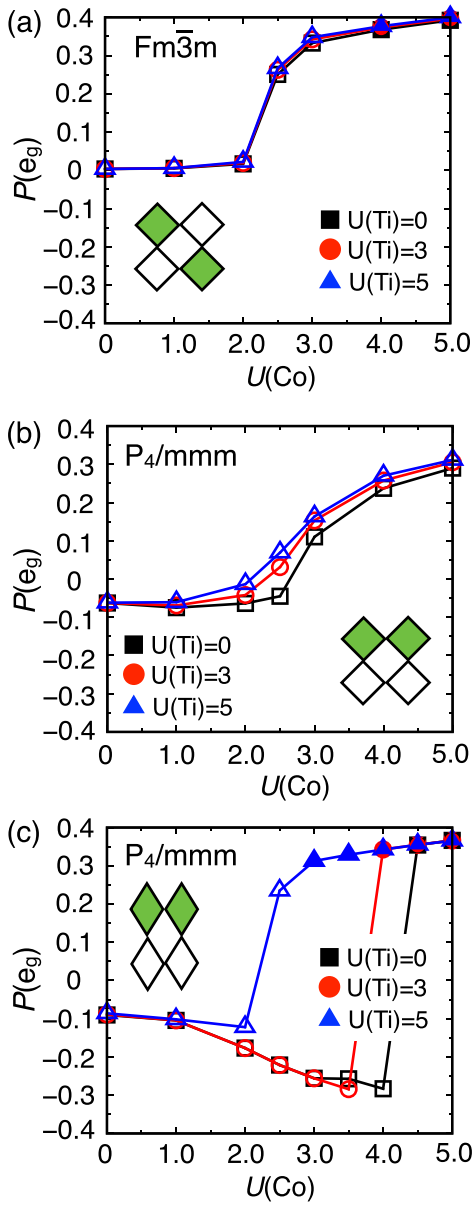

FIG. 6. (a)–(c) show the DFT+U orbital polarization $P(e_g)$ of the LS state structures with different space groups versus U(Co) and as a function of U(Ti) when the magnetic order between Co is antiferromagnetic (AFM). Empty and filled points indicate metallic and insulating phases, respectively. Insets show schematic side views of the octahedral tilts and distortions of the CoO_6 and TiO_6 oxygen octahedra.

the sign of P is not due to the space group symmetry reduction alone. Indeed, it is strongly determined by the local octahedral distortions, i.e., the relative in-plane and out-of-plane Co-O bond lengths. In the superlattice, the out-of-plane Co-O bond is well elongated by the local electric field between Co and Ti ions [53]. Since the Co has interfaces at both sides and thus both of its out-of-plane Co-O bonds are elongated, the octahedral distortion of CoO_6 in $(LCO)_1$+$(LTO)_1$ has standardized symmetry label $A_{1g} + E_g$ [57]. If the in-plane Co-O

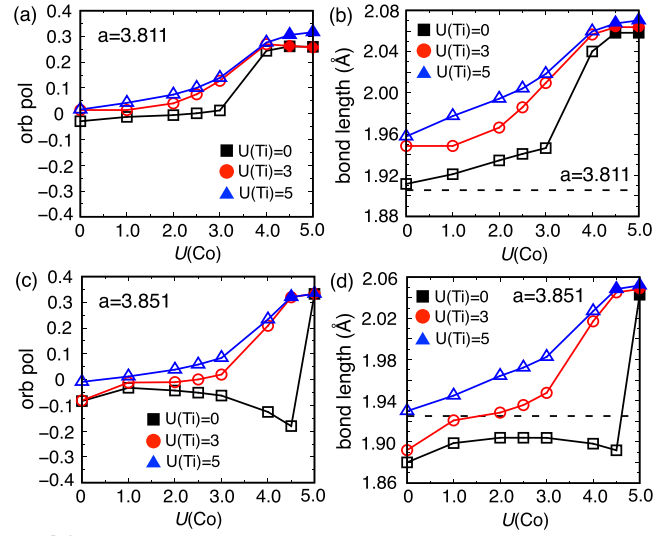

FIG. 7. (a),(c) Orbital polarization from DFT+U of the LCO+LTO superlattice (P_4/mmm, $a^0a^0a^0$, and $a = b \neq c$) with different in-plane lattice parameters. Empty and filled points indicate metallic and insulating phases, respectively. (b),(d) Out-of-plane Co-O bond lengths with different in-plane lattice parameters. Dashed lines represent the in-plane Co-O bond lengths, which are weak functions of U.

bond is longer than the out-of-plane Co-O bond, P becomes positive [Figs. 3(e) and 3(f)]. If the out-of-plane Co-O bond is longer than the in-plane Co-O bond, P becomes negative [Fig. 3(e)].

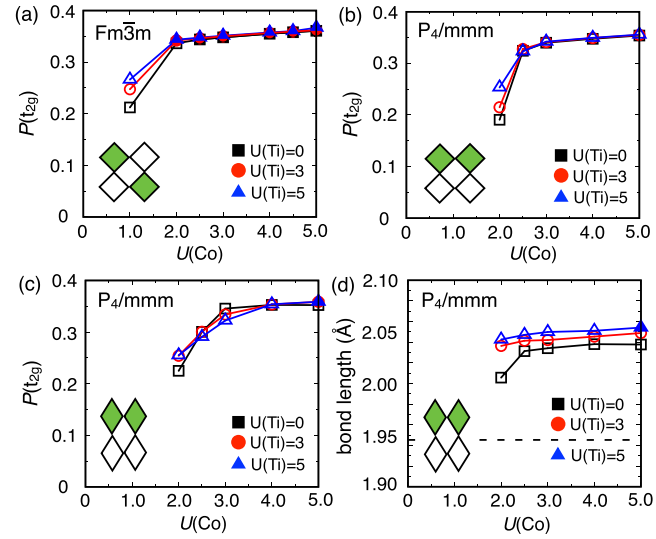

FIG. 8. (a)–(c) t_{2g} HS orbital polarization from DFT+U of the LCO+LTO heterostructures with different space groups; as shown by the insets, (b) has $a = b = c$ and (c) has $a = b \neq c$. Filled and empty points indicate metallic and insulating phases, respectively. (d) Out-of-plane Co-O bond lengths of the P_4/mmm phase with $a = b \neq c$. The dashed line represents the in-plane Co-O bond lengths, which are robust versus U.

TABLE III. Wannier Co d occupancies N_d for the high-spin states within DFT+DMFT calculations. The calculations use $U = 3$ eV, $J = 0.9$ eV, and a temperature of 300 K.

	d_{z^2}	$d_{x^2-y^2}$	d_{xy}	d_{xz}	d_{yz}
(i) $Fm\bar{3}m$ La_2CoTiO_6	1.00	1.00	1.67	1.67	1.67
(ii) $P4/mmm$ LCO+LTO ($a = b = c$)	1.00	1.00	1.00	2.00	2.00

3. LS e_g orbital polarization: Magnetic interactions

Thus far, we have discussed the origin of the orbital polarization where we have imposed ferromagnetic (FM) ordering of the Co cations. As we will see, the effect of different magnetic ordering might change the sign of the polarization, but it does not change any of our findings concerning the origin and magnitude of the orbital polarization.

To study the effect of the magnetic order on the polarization, we consider the antiferromagnetic (AFM) order for the $Fm\bar{3}m$ and $P4/mmm$ ($a = b = c$) phases using supercells containing two distinct Co atoms and compare to the FM phase. The DFT+U calculated orbital polarization is nonzero for the AFM $Fm\bar{3}m$ phase as shown in Fig. 6: Just like the FM phase, the DFT+U energy is minimized by spontaneous symmetry breaking. However, just like the FM phase, this is an artificial result, and quantum fluctuations should also wash out this orbital polarization.

The main reason is that the FM and AFM configurations are very close in energy, so that the actual system will be paramagnetic at any reasonable temperature. Due to the large distance between Co atoms in the double perovskite structure (larger than 5.5 Å) as per Fig. 2(a), the magnetic interaction between the Co cations is almost negligible: We find that the energies of the FM and AFM phases differ by only 0.3 meV/Co [for $U(\mathrm{Ti}) = 5$ eV and $U(\mathrm{Co}) = 5$ eV]. Hence, the system is essentially paramagnetic, and our explicit DFT+DMFT calculations for the paramagnetic phase found no orbital polarization.

The overall behavior of the polarization of the $P4/mmm$ structure with AFM ordering is also quite similar to the FM counterpart as shown in Figs. 6(b) and 6(c). Again, the structural symmetry reduction is the origin of the orbital polarization while U enhances the polarization strongly.

4. LS e_g orbital polarization: Strain dependence

Now we discuss the effect of the strain on the e_g orbital polarization for the LS phase. Since the sign and the magnitude of $P(e_g)$ depend on the relative sizes of the in-plane and out-of-plane Co-O bonds, strain can enhance, reduce, or change the sign of P, since the Co-O bond lengths can be strongly altered by the epitaxial strain. We consider the $P4/mmm$ ($a = b \neq c$) phase with in-plane lattice parameters of $a = 3.811$ and 3.851 Å and the results are summarized in Fig. 7 [the data for $a = 3.891$ Å is in Figs. 3(c) and 3(e)].

For $a = 3.811$ Å, where the CoO_6 octahedra feel compressive strain, apical Co-O bonds are always longer than the in-plane Co-O bonds. Thus, the d_{z^2} band is always lower in energy than the $d_{x^2-y^2}$ band, and $P > 0$ as per simple crystal field theory. In addition, $U_{\mathrm{Co}} > 0$ further increases the splitting between the e_g bands; as a result, both apical Co-O bond lengths and P are monotonically increasing functions of U_{Co}.

For $a = 3.851$ Å, which represents weaker compressive strain, the apical bonds are elongated but not always longer than the in-plane bonds. Therefore, similar to the $a = 3.891$ Å case, the sign of P depends on both U_{Co} and U_{Ti}. The biggest difference between $a = 3.851$ and 3.891 Å is evident for the ($U_{\mathrm{Co}} = 5$, $U_{\mathrm{Ti}} = 0$) case: $P > 0$ for $a = 3.851$ Å but $P < 0$ for $a = 3.891$ Å.

D. HS state: t_{2g} orbital polarization

In this section, we consider the orbital polarization of the t_{2g} bands, the relevant quantity for the HS Co^{2+} spin state. In prior work, we showed that large tensile strain stabilizes antiferro-orbital ordering in the HS $P2_1/n$ phase [53]. However, for the range of in-plane lattice parameters considered here, the antiferro-orbital ordering is almost negligible: The magnitude of the JT distortion (difference between two in-plane Co-O bonds) is less than 0.007 Å. For what follows below, we average the orbital polarization of two Co atoms, but we note that this averaged value and the separate values from either Co atom are almost identical.

We define the orbital polarization of the high-spin (HS) state as

$$P(t_{2g}) = \frac{(n^{\uparrow}_{xz} + n^{\downarrow}_{xz}) + (n^{\uparrow}_{yz} + n^{\downarrow}_{yz}) - 2(n^{\uparrow}_{xy} + n^{\downarrow}_{xy})}{(n^{\uparrow}_{xz} + n^{\downarrow}_{xz}) + (n^{\uparrow}_{yz} + n^{\downarrow}_{yz}) + 2(n^{\uparrow}_{xy} + n^{\downarrow}_{xy})}. \quad (4)$$

We consider three structures: (i) $Fm\bar{3}m$ space group and $a^0a^0a^0$ tilt, (ii) $P4/mmm$ with $a = b = c$, and (iii) $P4/mmm$ with $a = b \neq c$. We do not examine the $P2_1/n$ case: The local t_{2g} states on each Co become mixed due to the octahedral tilts, and the off-diagonal elements of the density matrix in the t_{2g} manifold become large and non-negligible: This makes unambiguous extraction of individual orbital occupancies difficult.

Figure 8(a) shows that P for the highest symmetry $Fm\bar{3}m$ structure is generally nonzero for even modest U_{Co} values: This means that the t_{2g} subsystem has a stronger propensity to spontaneously break electronic symmetry at the DFT+U level when compared to the e_g system above. We believe this is due to the narrower t_{2g} energy bands and the more localized electronic states on the Co cations. However, the total energies of the three equivalent configurations $d^1_{xy\downarrow}d^1_{xz\downarrow}d^0_{yz\downarrow}$, $d^1_{xy\downarrow}d^0_{xz\downarrow}d^1_{yz\downarrow}$, and $d^0_{xy\downarrow}d^1_{xz\downarrow}d^1_{yz\downarrow}$ differ by only 0.1 meV/Co (see Table I). Again, this indicates that the actual interacting $Fm\bar{3}m$ system should have significant fluctuations between these configurations and zero mean orbital polarization. Next, in both $P4/mmm$ phases, we expect the orbital polarization predicted in Figs. 8(b) and 8(c) to be observable because, as Table I shows, the $d^0_{xy\downarrow}d^1_{xz\downarrow}d^1_{yz\downarrow}$ configuration has significantly lower energy than the other competing configurations (which are antiferro-orbital ordered with alternating $d^1_{xy\downarrow}d^1_{xz\downarrow}d^0_{yz\downarrow}$ and $d^1_{xy\downarrow}d^0_{xz\downarrow}d^1_{yz\downarrow}$ configurations).

Permitting the local octahedra to elongate in going from the $P4/mmm$ $a = b = c$ to the $a = b \neq c$ phase [Fig. 8(b) to Fig. 8(c)] increases the polarization P. The main difference from the e_g case is that the sign of P is insensitive to the value of both U_{Co} and U_{Ti}. This goes hand in hand with the structure of the system: Figure 8(d) shows that the HS t_{2g} system has

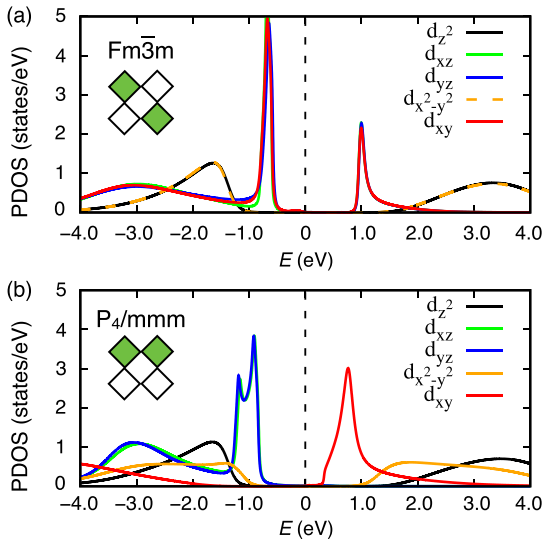

FIG. 9. DFT+DMFT spectral functions of Co d Wannier orbitals for (a) HS La_2CoTiO_6 ($Fm\bar{3}m$) and (b) the HS LTO+LCO superlattice (P_4/mmm, $a = b = c$). The calculations use $U = 3$ eV, $J = 0.9$ eV, and a temperature of 300 K.

longer out-of-plane Co-O bonds than the e_g LS case, and its out-of-plane bonds are always longer than the in-plane bonds.

To study the importance of quantum fluctuations, we repeat our procedure for the LS phases. We employ DFT+DMFT calculations for the HS states of La_2CoTiO_6 ($Fm\bar{3}m$ structure) and LTO+LCO superlattice (P_4/mmm, $a = b = c$ structure), and the results are summarized in Fig. 9 and Table III (we use a larger value of $J = 0.9$ eV to stabilize the HS spin configuration). Much like the LS case, the HS $Fm\bar{3}m$ phase retains its t_{2g} degeneracy within DFT+DMFT due to the quantum fluctuation between the t_{2g} orbitals and shows no orbital polarization. On the other hand, for the HS P_4/mmm phase, the t_{2g} bands split into doubly-degenerate d_{xz}+d_{yz} bands and nondegenerate d_{xy} band as shown in Fig. 9(b): The superlatticing effect is sufficient to generate and stabilize the orbital polarization.

IV. SUMMARY

In this work, we have shown that orbital polarization in the cobaltate systems we have studied has its fundamental origin in the structure and symmetry of the material (the crystalline environment of the Co cations); strong electronic interactions can enhance the polarization but are not necessary to generate it. Specifically, the requisite symmetry reduction does not require local octahedral distortions about the Co cations: The formation of a superlattice by itself is sufficient to generate orbital polarization by breaking electronic symmetry within the Co e_g and t_{2g} manifolds. In comparison, in bulk perovskites, local octahedral deformations such as Jahn-Teller (JT) distortions are needed for structural symmetry reduction which leads to broken electronic symmetry and orbital polarization. In fact, the role of the oxygen octahedral elongation turns out to be similar to the role of the electronic interactions: It is not needed to create the polarization but enhances it significantly.

We also find that in the highest symmetry structural phases ($Fm\bar{3}m$), DFT+U predicts a broken symmetry solutions of unequal orbital occupancies and orbital polarization. However, this electronic symmetry breaking is artificial, and DFT+DMFT calculations that can include quantum fluctuations between different configurations, which are missing in DFT+U, lead to zero orbital polarization.

We note that the structural symmetry breaking modes considered here are simple and in some sense crude: They break symmetry in both the e_g and t_{2g} manifolds and are unable to selectively do so in one or the other manifold. In principle, we can envision symmetry breaking operations that selectively remove degeneracy in only one manifold, but they will require control over the electronic potential in a fine-grained microscopic manner that goes beyond simply distorting cation-oxygen bonds. Whether such an advanced level of control is feasible in actual materials is, in our mind, an interesting open question.

ACKNOWLEDGMENTS

We thank Sangjae Lee, F. J. Walker, and Charles H. Ahn for helpful discussions. We thank the Yale Center for Research Computing for guidance and use of the research

TABLE IV. Eigenvalues (ν_i, last column) and eigenvector components squared (probabilities) of the 10 × 10 single-particle density matrix of the Co 3d manifold obtained within GGA+U+SOC calculations. Structural phase is P_4/mmm ($a = b \neq c$) with $U_{\mathrm{Ti}} = 5$ eV and $U_{\mathrm{Co}} = 5$ eV and LS cobalt spin state. Each row describes one eigenvalue/eigenvector.

	$d^{\uparrow}_{xy}$	$d^{\uparrow}_{yz}$	$d^{\uparrow}_{z^2}$	$d^{\uparrow}_{xz}$	$d^{\uparrow}_{x^2-y^2}$	$d^{\downarrow}_{xy}$	$d^{\downarrow}_{yz}$	$d^{\downarrow}_{z^2}$	$d^{\downarrow}_{xz}$	$d^{\downarrow}_{x^2-y^2}$	ν_i
ν_1	0.000	0.046	0.000	0.046	0.000	0.002	0.000	0.000	0.000	0.906	0.146
ν_2	0.000	0.000	0.000	0.000	0.000	0.000	0.000	1.000	0.000	0.000	0.156
ν_3	0.003	0.000	0.000	0.000	0.997	0.000	0.000	0.000	0.000	0.000	0.393
ν_4	0.000	0.000	0.053	0.000	0.000	0.000	0.473	0.000	0.473	0.000	0.865
ν_5	0.002	0.000	0.000	0.000	0.000	0.000	0.499	0.000	0.499	0.000	0.947
ν_6	0.000	0.040	0.000	0.040	0.000	0.918	0.000	0.000	0.000	0.002	0.952
ν_7	0.000	0.500	0.000	0.500	0.000	0.000	0.000	0.000	0.000	0.000	0.958
ν_8	0.995	0.000	0.000	0.000	0.003	0.000	0.001	0.000	0.001	0.000	0.968
ν_9	0.000	0.000	0.947	0.000	0.000	0.000	0.027	0.000	0.027	0.000	1.023
ν_{10}	0.000	0.414	0.000	0.414	0.000	0.079	0.000	0.000	0.000	0.092	1.047

computing infrastructure. This work also used the Extreme Science and Engineering Discovery Environment (XSEDE), which is supported by National Science Foundation Grant No. ACI-1548562, by using computer time on the Comet supercomputer as enabled by XSEDE allocation MCA08X007. H.P. is supported by NSF SI2-SSE Grant No. 1740112.

APPENDIX A: EFFECT OF SOC

It is known that the strength of the spin-orbit coupling (SOC) is small for transition metal $3d$ orbitals [58]. For Co, experiments show that the SOC constant of Co^{2+} is 16 meV [59]. Given that the SOC is weak for Co^{2+}, we expect a very weak SOC effect on the orbital polarization, and thus we check only a few cases using GGA+U+SOC calculations. Since SOC will break the block diagonal structure of the single-particle density matrix in the spin sector, we use the eigenvalues of the single-particle density matrix of the entire Co $3d$ manifold.

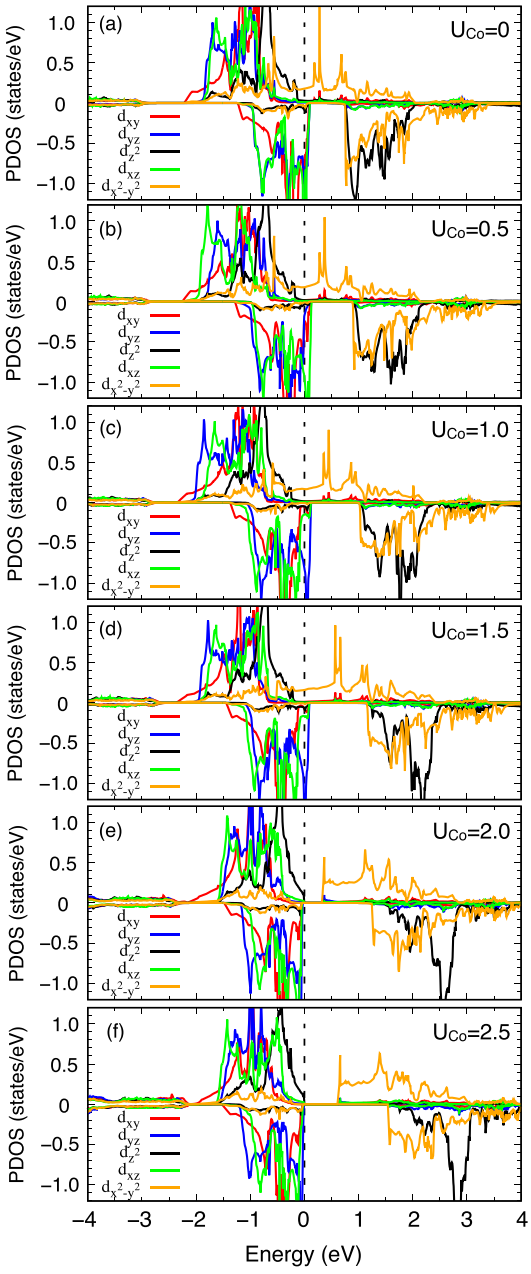

FIG. 10. (a)–(f) Co $3d$ projected density of states for low-spin (LS) Co in the $(LaCoO_3)_1 + (LaTiO_3)_1$ superlattice as a function of U_{Co} in eV. The value of U_{Ti} is 5 eV, the in-plane lattice parameters a and b are fixed to 3.811 Å, and the atomic structure has the $P2_1/n$ space group.

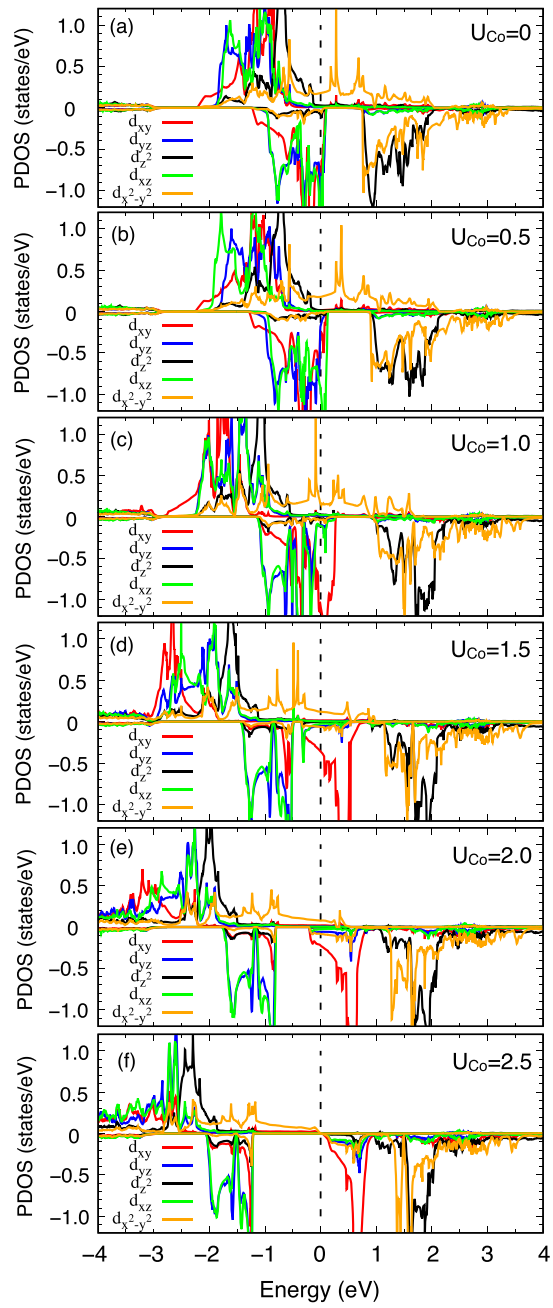

FIG. 11. (a)–(f) Co $3d$ projected density of states of high-spin (HS) Co in the $(LaCoO_3)_1 + (LaTiO_3)_1$ superlattice as a function of U_{Co} in eV. The value of U_{Ti} is 5 eV, the in-plane lattice parameters a and b are fixed to 3.811 Å, and the atomic structure has the $P2_1/n$ space group. Note that for $U_{Co} = 0$ and 0.5, the HS state is not even metastable, so the Co has the LS state. The in-plane lattice parameters a and b are fixed to 3.811 Å.

For e_g polarization, we choose four eigenvectors where the largest portion is $d_{z^2}^{\uparrow}$, $d_{z^2}^{\downarrow}$, $d_{x^2-y^2}^{\uparrow}$, and $d_{x^2-y^2}^{\downarrow}$, respectively, and use their eigenvalues to calculate the polarization. For example, for the $P4/mmm$ ($a = b \neq c$) LS phase with $U_{\mathrm{Ti}} = 5$ eV and $U_{\mathrm{Co}} = 5$ eV, the polarization within SOC $P_{\mathrm{soc}}(e_g)$ is obtained by

$$P_{\mathrm{soc}}(e_g) = \frac{(\nu_9 + \nu_2) - (\nu_3 + \nu_1)}{(\nu_9 + \nu_2) + (\nu_3 + \nu_1)}, \tag{A1}$$

where ν_i are related eigenvalues among the 10×10 single-particle density matrix for the case of d electrons, shown in Table IV. Not surprisingly given the weak SOC strength for the $3d$ orbital, in this case the polarizations with and without SOC are $P(e_g) = 0.349$ and $P_{\mathrm{soc}}(e_g) = 0.344$, respectively, which differ by $\sim 1\%$.

APPENDIX B: PDOS

The figures in this Appendix (Figs. 10–17) provide the projected densities of electronic states for many of the systems described in the main text.

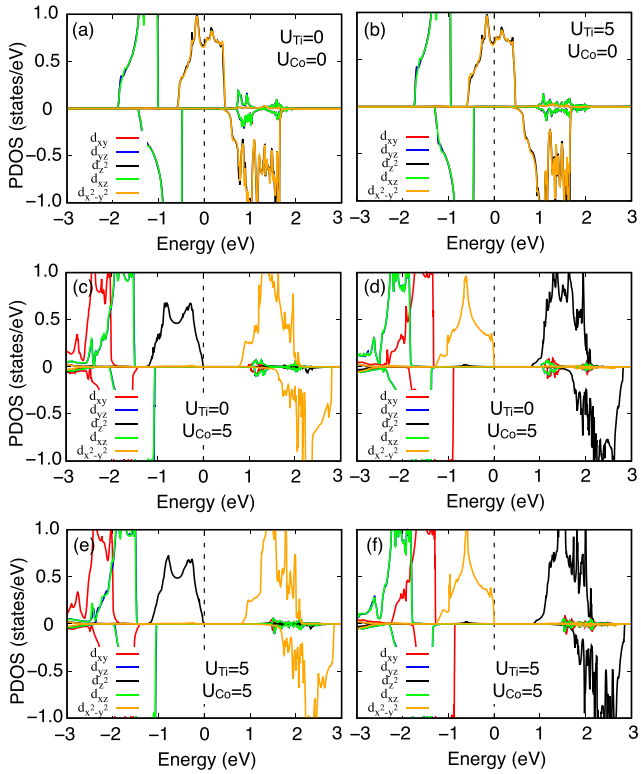

FIG. 12. Comparison of the Co $3d$ projected density of states of the two different self-consistent solutions for low-spin (LS) Co in the double perovskite La_2TiCoO_6 (cubic, $Fm\bar{3}m$ space group) as a function of U_{Co} and U_{Ti} in eV. (c) and (e) are for the d_{z^2}-occupied LS states, and (d) and (f) are for the $d_{x^2-y^2}$-occupied LS states. Lattice parameters are fixed to $a = b = c = 3.891$ Å, obtained by minimizing the stress of La_2TiCoO_6 with $U_{\mathrm{Co}} = U_{\mathrm{Ti}} = 3$.

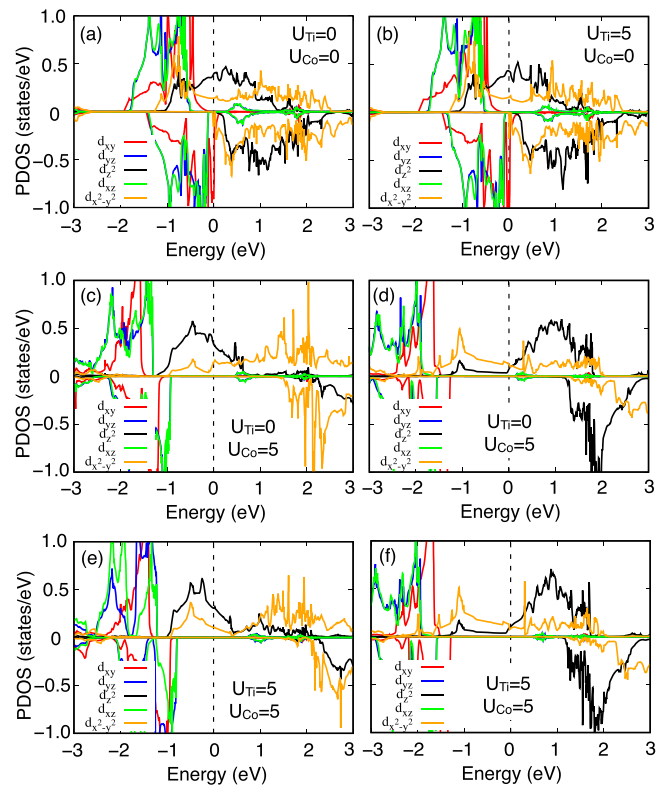

FIG. 13. Comparison of the Co $3d$ projected density of states of the two different self-consistent solutions for low-spin (LS) Co in the $(LaCoO_3)_1 + (LaTiO_3)_1$ superlattice ($P4/mmm$ space group, $a = b = c$) as a function of U_{Co} and U_{Ti} in eV. (c) and (e) are for the d_{z^2}-occupied LS states, and (d) and (f) are for the $d_{x^2-y^2}$-occupied LS states. Lattice parameters are fixed to $a = b = c = 3.891$ Å.

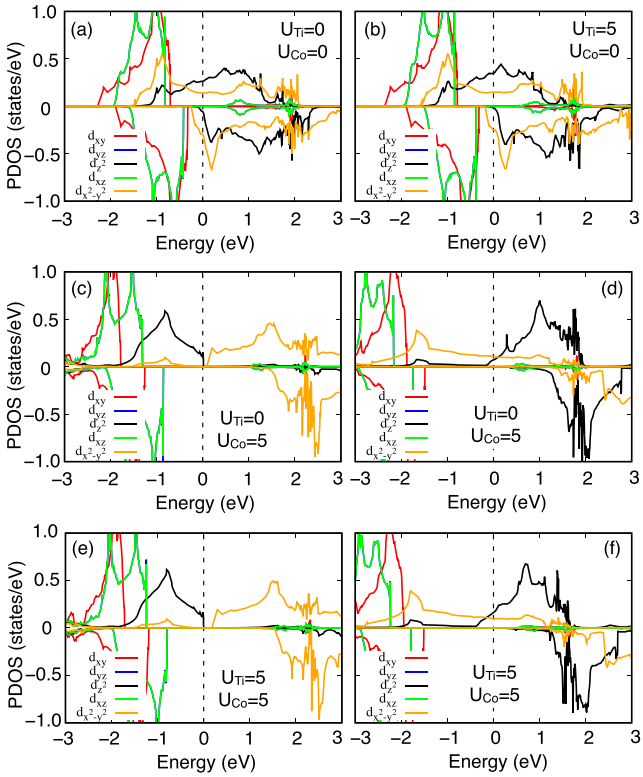

FIG. 14. Comparison of the Co $3d$ projected density of states of the two different self-consistent solutions for low-spin (LS) Co in $(LaCoO_3)_1 + (LaTiO_3)_1$ (P_4/mmm space group, $a = b \neq c$) as a function of U_{Co} and U_{Ti} in eV. (c) and (e) are for the d_{z^2}-occupied LS states, and (d) and (f) are for the $d_{x^2-y^2}$-occupied LS states. In-plane lattice parameters are fixed to $a = b = 3.891$ Å, while c is different due to the relaxation.

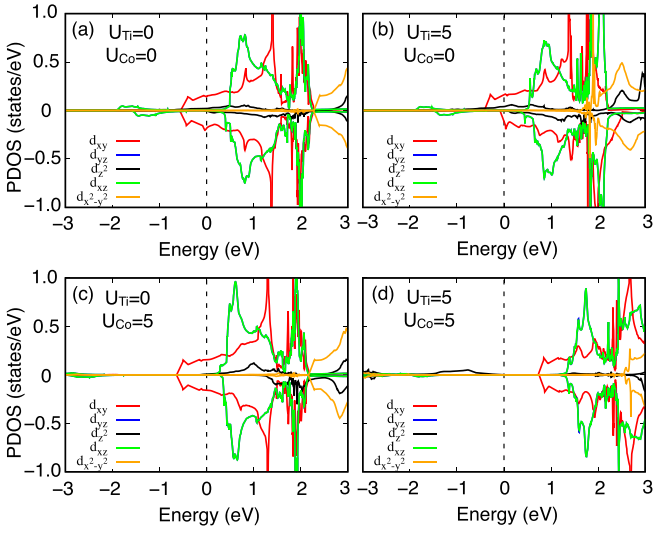

FIG. 15. Ti $3d$ projected density of states for the low-spin (LS) Co in the $(LaCoO_3)_1 + (LaTiO_3)_1$ superlattice (P_4/mmm space group, $a = b \neq c$) as a function of U_{Co} and U_{Ti} in eV. In-plane lattice parameters are fixed to $a = b = 3.891$ Å, while c is different due to the relaxation.

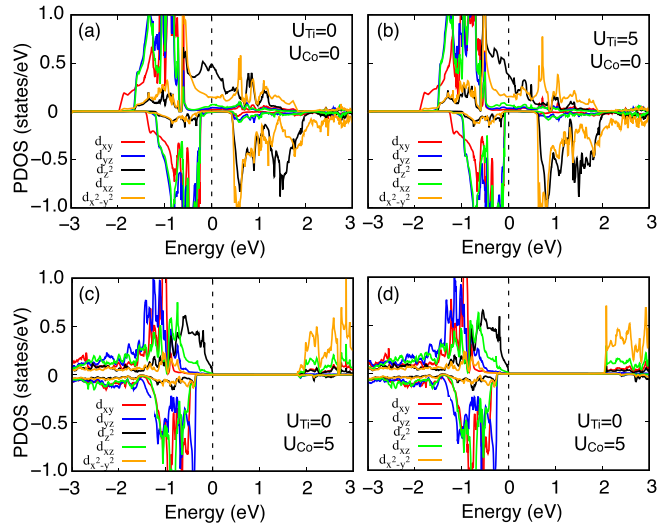

FIG. 16. Co $3d$ projected density of states for the low-spin (LS) Co in the $(LaCoO_3)_1 + (LaTiO_3)_1$ superlattice ($P2_1/n$ space group, $a = b \neq c$) as a function of U_{Co} and U_{Ti} in eV. In-plane lattice parameters are fixed to $a = b = 3.891$ Å, while c is different due to the relaxation.

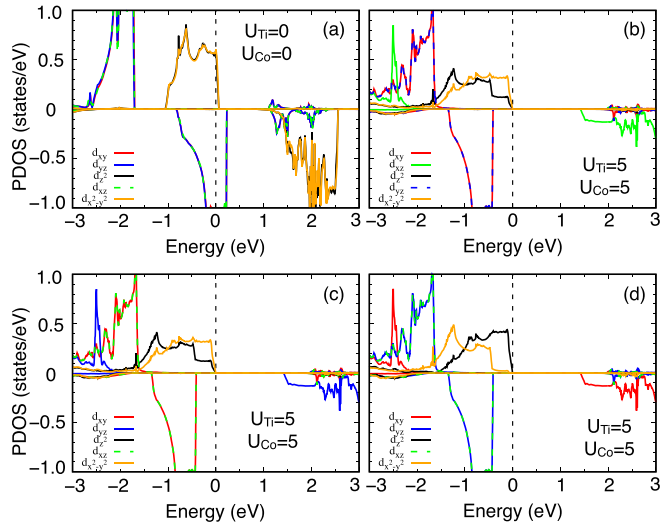

FIG. 17. Co $3d$ projected density of states (PDOS) for high-spin (HS) Co in the double perovskite La_2TiCoO_6 (cubic, $Fm\bar{3}m$ space group) as a function of U_{Co} and U_{Ti} in eV. (a) For $U_{Ti} = U_{Co} = 0$, the minority (down) t_{2g} states are equally occupied showing no orbital polarization. For $U_{Ti} = U_{Co} = 5$ eV, three physically equivalent different minority t_{2g} configurations can be stabilized: (b) $d^1_{xy\downarrow} d^0_{xz\downarrow} d^1_{yz\downarrow}$, (c) $d^1_{xy\downarrow} d^1_{xz\downarrow} d^0_{yz\downarrow}$, and (d) $d^0_{xy\downarrow} d^1_{xz\downarrow} d^1_{yz\downarrow}$. Lattice parameters are fixed to $a = b = c = 3.891$ Å.

[1] P. A. Lee, N. Nagaosa, and X.-G. Wen, Rev. Mod. Phys. **78**, 17 (2006).
[2] E. Dagotto, Rev. Mod. Phys. **66**, 763 (1994).
[3] A. Damascelli, Z. Hussain, and Z.-X. Shen, Rev. Mod. Phys. **75**, 473 (2003).
[4] F. C. Zhang and T. M. Rice, Phys. Rev. B **37**, 3759 (1988).
[5] Y. Konishi, Z. Fang, M. Izumi, T. Manako, M. Kasai, H. Kuwahara, M. Kawasaki, K. Terakura, and Y. Tokura, J. Phys. Soc. Jpn. **68**, 3790 (1999).
[6] Y. Tokura and N. Nagaosa, Science **288**, 462 (2000).
[7] B. R. K. Nanda and S. Satpathy, Phys. Rev. B **81**, 174423 (2010).
[8] D. Pesquera, G. Herranz, A. Barla, E. Pellegrin, F. Bondino, E. Magnano, F. Sánchez, and J. Fontcuberta, Nat. Commun. **3**, 1189 (2012).
[9] M. Imada, A. Fujimori, and Y. Tokura, Rev. Mod. Phys. **70**, 1039 (1998).
[10] M. W. Haverkort, Z. Hu, A. Tanaka, W. Reichelt, S. V. Streltsov, M. A. Korotin, V. I. Anisimov, H. H. Hsieh, H.-J. Lin, C. T. Chen *et al.*, Phys. Rev. Lett. **95**, 196404 (2005).
[11] A. T. Lee and C. A. Marianetti, Phys. Rev. B **97**, 045102 (2018).
[12] C. Zobel, M. Kriener, D. Bruns, J. Baier, M. Grüninger, T. Lorenz, P. Reutler, and A. Revcolevschi, Phys. Rev. B **66**, 020402(R) (2002).
[13] H. Park, R. Nanguneri, and A. T. Ngo, Phys. Rev. B **101**, 195125 (2020).
[14] H. Y. Hwang, Y. Iwasa, M. Kawasaki, B. Keimer, N. Nagaosa, and Y. Tokura, Nat. Mater. **11**, 103 (2012).
[15] H. A. Jahn and E. Teller, Proc. R. Soc. Lond. A **161**, 220 (1937).
[16] J. B. Goodenough, Phys. Rev. **100**, 564 (1955).
[17] J. B. Goodenough, J. Phys. Chem. Solids **6**, 287 (1958).
[18] J. Kanamori, J. Phys. Chem. Solids **10**, 87 (1959).
[19] K. I. Kugel' and D. I. Khomskiĭ, Soviet Physics Uspekhi **25**, 231 (1982).
[20] J. P. Wright, J. P. Attfield, and P. G. Radaelli, Phys. Rev. B **66**, 214422 (2002).
[21] J. Schlappa, C. Schüßler-Langeheine, C. F. Chang, H. Ott, A. Tanaka, Z. Hu, M. W. Haverkort, E. Schierle, E. Weschke, G. Kaindl *et al.*, Phys. Rev. Lett. **100**, 026406 (2008).
[22] I. Leonov, A. N. Yaresko, V. N. Antonov, M. A. Korotin, and V. I. Anisimov, Phys. Rev. Lett. **93**, 146404 (2004).
[23] K. Yamauchi, T. Fukushima, and S. Picozzi, Phys. Rev. B **79**, 212404 (2009).
[24] M. S. Senn, J. P. Wright, and J. P. Attfield, Nature **481**, 173 (2012).
[25] A. Tebano, C. Aruta, S. Sanna, P. G. Medaglia, G. Balestrino, A. A. Sidorenko, R. De Renzi, G. Ghiringhelli, L. Braicovich, V. Bisogni *et al.*, Phys. Rev. Lett. **100**, 137401 (2008).
[26] A. Tebano, A. Orsini, P. G. Medaglia, D. Di Castro, G. Balestrino, B. Freelon, A. Bostwick, Y. J. Chang, G. Gaines, E. Rotenberg *et al.*, Phys. Rev. B **82**, 214407 (2010).
[27] H. Chen, D. P. Kumah, A. S. Disa, F. J. Walker, C. H. Ahn, and S. Ismail-Beigi, Phys. Rev. Lett. **110**, 186402 (2013).
[28] A. S. Disa, D. P. Kumah, A. Malashevich, H. Chen, D. A. Arena, E. D. Specht, S. Ismail-Beigi, F. J. Walker, and C. H. Ahn, Phys. Rev. Lett. **114**, 026801 (2015).
[29] S. Lee, A. T. Lee, A. B. Georgescu, G. Fabbris, M.-G. Han, Y. Zhu, J. W. Freeland, A. S. Disa, Y. Jia, M. P. M. Dean *et al.*, Phys. Rev. Lett. **123**, 117201 (2019).
[30] V. G. Bhide, D. S. Rajoria, G. R. Rao, and C. N. R. Rao, Phys. Rev. B **6**, 1021 (1972).
[31] K. Asai, O. Yokokura, N. Nishimori, H. Chou, J. M. Tranquada, G. Shirane, S. Higuchi, Y. Okajima, and K. Kohn, Phys. Rev. B **50**, 3025 (1994).
[32] M. Itoh, I. Natori, S. Kubota, and K. Motoya, J. Phys. Soc. Jpn. **63**, 1486 (1994).
[33] R. H. Potze, G. A. Sawatzky, and M. Abbate, Phys. Rev. B **51**, 11501 (1995).
[34] T. Saitoh, T. Mizokawa, A. Fujimori, M. Abbate, Y. Takeda, and M. Takano, Phys. Rev. B **55**, 4257 (1997).
[35] K. Asai, A. Yoneda, O. Yokokura, J. M. Tranquada, G. Shirane, and K. Kohn, J. Phys. Soc. Jpn. **67**, 290 (1998).
[36] S. Yamaguchi, Y. Okimoto, and Y. Tokura, Phys. Rev. B **55**, R8666 (1997).
[37] A. I. Liechtenstein, V. I. Anisimov, and J. Zaanen, Phys. Rev. B **52**, R5467 (1995).
[38] P. E. Blöchl, Phys. Rev. B **50**, 17953 (1994).
[39] J. P. Perdew, A. Ruzsinszky, G. I. Csonka, O. A. Vydrov, G. E. Scuseria, L. A. Constantin, X. Zhou, and K. Burke, Phys. Rev. Lett. **100**, 136406 (2008).
[40] G. Kresse and D. Joubert, Phys. Rev. B **59**, 1758 (1999).
[41] P. M. Woodward, Acta Crystallographica Section B **53**, 32 (1997).
[42] H. Park, A. J. Millis, and C. A. Marianetti, Phys. Rev. B **92**, 035146 (2015).
[43] J. Chen, A. J. Millis, and C. A. Marianetti, Phys. Rev. B **91**, 241111(R) (2015).
[44] H. Chen and A. J. Millis, Phys. Rev. B **93**, 045133 (2016).
[45] O. Bengone, M. Alouani, P. Blöchl, and J. Hugel, Phys. Rev. B **62**, 16392 (2000).
[46] A. Rohrbach, J. Hafner, and G. Kresse, J. Phys.: Condens. Matter **15**, 979 (2003).
[47] V. Singh, U. Herath, B. Wah, X. Liao, A. H. Romero, and H. Park, Comput. Phys. Commun. **261**, 107778 (2021).
[48] N. Marzari, A. A. Mostofi, J. R. Yates, I. Souza, and D. Vanderbilt, Rev. Mod. Phys. **84**, 1419 (2012).
[49] K. Haule, Phys. Rev. B **75**, 155113 (2007).
[50] E. Gull, A. J. Millis, A. I. Lichtenstein, A. N. Rubtsov, M. Troyer, and P. Werner, Rev. Mod. Phys. **83**, 349 (2011).
[51] M. Karolak, M. Izquierdo, S. L. Molodtsov, and A. I. Lichtenstein, Phys. Rev. Lett. **115**, 046401 (2015).
[52] V. I. Anisimov, J. Zaanen, and O. K. Andersen, Phys. Rev. B **44**, 943 (1991).
[53] A. T. Lee and S. Ismail-Beigi, Phys. Rev. B **101**, 144423 (2020).
[54] H. Park, A. J. Millis, and C. A. Marianetti, Phys. Rev. Lett. **109**, 156402 (2012).
[55] K. Haule and G. L. Pascut, Sci. Rep. **7**, 10375 (2017).
[56] E. Greenberg, I. Leonov, S. Layek, Z. Konopkova, M. P. Pasternak, L. Dubrovinsky, R. Jeanloz, I. A. Abrikosov, and G. K. Rozenberg, Phys. Rev. X **8**, 031059 (2018).
[57] X. Ai, Y. Chen, and C. A. Marianetti, Phys. Rev. B **90**, 014308 (2014).
[58] G. M. Cole and B. B. Garrett, Inorganic Chemistry **9**, 1898 (1970).
[59] R. A. Cowley, W. J. L. Buyers, C. Stock, Z. Yamani, C. Frost, J. W. Taylor, and D. Prabhakaran, Phys. Rev. B **88**, 205117 (2013).